Optimal Photon Counting Receiver for Sub-Dead-Time Signal Transmission

Optimal Photon Counting Receiver for Sub-Dead-Time Signal Transmission

Shenjie Huang, Sarrah M. Patanwala, John Kosman, Robert K. Henderson, and Majid Safari

***Abstract*—In many practical scenarios, single-photon avalanche diodes (SPADs) are good solutions to improve the performance of optical communication systems due to their high sensitivity to photon arrival. SPAD receivers can be implemented in large arrays to achieve higher data rates and additional protection against background light; however, they suffer from a significant intersymbol interference (ISI) if the SPAD dead time is comparable or larger than the symbol duration, i.e., sub-dead-time signal transmission. This work proposes a novel detection scheme designed for high-speed SPAD-based systems to effectively mitigate the degradation induced by ISI. Different from traditional receivers, in the proposed scheme, the information extracted from both the counts and arrival times of photons are utilised for the optimal symbol detection in the presence of the non-linear and random ISI effect due to dead time. Our extensive numerical and experimental results demonstrate the superiority of the proposed photon time information based detection (PTID) scheme in terms of both BER performance and background light tolerance of the communication link. In addition, a linear approximation of the SPAD-based channel is investigated, which illustrates that the traditional equalization methods are effective under some specific circumstances.**

I. Introduction

In recent decades, there has been a growing interest in employing photon counting detectors in both fiber [2] and optical wireless communication (OWC) systems [3], [4] to improve the sensitivity of receivers. To realize a photon counting receiver, the commonly used avalanche photodiode (APD) can be biased above the breakdown voltage so that it operates at Geiger mode. By doing so, a single-photon counting avalanche diode (SPAD) can be achieved which has the advantages of single photon sensitivity and picosecond temporal resolution. Large arrays of SPADs that can be employed for imaging and high-speed communication applications are now commercially available. In [3], A reconfigurable SPAD receiver is designed for OWC systems with a sensitivity of -31.7 dBm at 100 Mbit/s and 450 nm. In [2], the experimental results of a SPAD-based optical fiber receiver are presented and a measurement of -55.7 dBm and -51.6 dBm sensitivities at a data rate of 50 Mbit/s and 100 Mbit/s for a BER of 2×10^{-3} is achieved. However, the corresponding quantum limits are -73 dBm and -70 dBm, respectively. Therefore, the sensitivities of the currently available SPAD receivers are still far away from the quantum limit, which is mainly due to the limited fill-factor and photon detection probability (PDP). In addition, the achievable data rate of the SPAD-based communication systems is strongly limited by the signal nonlinearity caused by *dead time* when SPADs become inactive for a period of several nanoseconds [5]. The dead time typically happens following the avalanche caused by each photon detection when the SPAD is getting quenched. There are two types of quenching circuits in SPAD receivers, i.e., active quenching (AQ) and passive quenching (PQ). The dead time of AQ SPADs is constant, whereas for PQ SPADs the photons arriving during the dead time can extend its duration [6].

In the literature, the performance degradation of SPAD-based communication systems introduced by dead time is not well investigated. Some studies assume that the received photon count is an ideal Poisson distributed random variable (RV) with the incident photon rate as its mean. However, this model completely ignores the dead time effect and as a result the BER performance is significantly overestimated as shown in [4]. Some other works employ the effects of dead time by assuming that the detected photon count is a Poisson random variable with an effective average rate defined based on the dead time [7], [8]. There are two issues regarding this assumption. Firstly, these effective rates are derived based on the renewal theory assuming that the incident photon rate is fixed [9], therefore they are approximately accurate only when the symbol duration is much longer than dead time. For high speed *sub-dead-time* data transmission where the symbol time is even less than the dead time, such approximation is not valid [10]. Secondly, by using this assumption, the intersymbol interference (ISI) caused by dead time is ignored. In practical high speed SPAD-based systems, the effect of dead time is more crucial particularly when the dead time started in a symbol extends to the subsequent symbols causing an ISI effect that cannot be ignored.

In [10], the accurate probability mass functions (PMFs) of the detected photon counts for both PQ and AQ SPADs have been derived; however, in this work the ISI effect is also ignored by assuming that the SPAD is always active at the beginning of each symbol duration to simplify the mathematical derivations. To mitigate the ISI induced by dead time, the SPAD receivers are usually operated under the condition that the symbol time is longer than or approximately equal to the dead time [11]. For high-speed sub-dead-time SPAD-based systems, some equalization methods, e.g., linear equalizer [5] and decision-feedback (DFE) equalizer [11], [12], originally designed for RF systems with linear channel expressions have been applied to SPAD-based OWC systems; however, SPAD-based channels are inherently nonlinear and require novel detection techniques to reduce the impacts of ISI based on the special characteristics of SPADs, which is

The authors are with the School of Engineering, the University of Edinburgh, Edinburgh EH9 3JL, U.K. (e-mail: {shenjie.huang}@ed.ac.uk).

This paper was presented in part at ECOC 2019 [1].

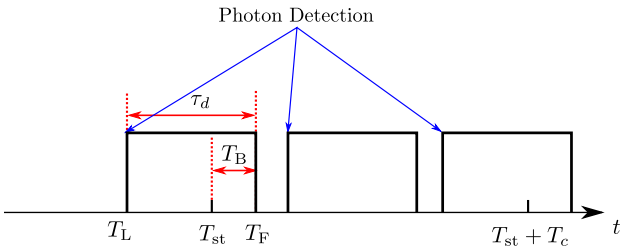

Fig. 1. The photon arrival sequence where T_L is the last photon arrival time before the considered symbol, $T_{\rm st}$ and $T_{\rm st}+T_{\rm c}$ denote the start and the end of the symbol, respectively, T_c refers to the symbol duration, and $T_{\rm F}$ is the end of the avalanche caused by the photon arrives at T_L.

still a research gap in the literature to the best of authors' knowledge.

SPADs can provide not only the photon count but also the accurate photon arrival time information, which we term as photon time information (PTI) [13], [14]. However, most of the works investigating the application of SPAD in communication only focus on its photon counting capability [3], [11]. Inspired by time-correlated single photon counting (TCSPC) techniques, a time correlation encoding method is considered in [14] which explores SPAD's capability of recording photon arrival times. Although such system has good resilience to background light, its achievable data rate is quite limited. In our recent work [1], a novel detection technique for SPAD-based sub-dead-time communication systems using both the photon count and the PTI is proposed and through the numerical results, the effectiveness of the proposed detection method is demonstrated. In this work, we extend the work [1] by further investigating the application of the proposed technique in the systems with large SPAD array. In addition, the effectiveness of the traditional equalization methods in SPAD-based systems is also discussed. Furthermore, using the SPAD receiver presented in [15], the performance improvement of the proposed technique is also demonstrated experimentally.

The rest of this paper is organized as follows. The effect of ISI is shown in Section II. The proposed ISI mitigation method is presented in Section III. The linear approximation of the SPAD channel is investigated in Section IV. Later, the numerical results and discussion are presented in Section V and the experimental results are shown in Section VI. Finally, we conclude this paper in Section VII.

II. Photon Counting in the Presence of ISI

Since SPAD is extremely sensitive to photon arrivals, when a photon triggers an avalanche event, an electrical pulse signal at the output of SPAD can be detected. However, due to the existence of dead time, the SPAD remains blind to the incident photons for a short period of time after a photon is detected. An example of the detected photon arrival sequence is plotted in Fig. 1, where each pulse is generated by a photon detection. The AQ SPAD has a fixed dead time τ_d and hence the output pulse width is fixed; whereas, the dead time of the PQ SPAD extends when extra photons arrive during the dead time. Therefore, for PQ SPAD, the pulse width is not fixed but the minimum pulse width would be still equivalent to τ_d.

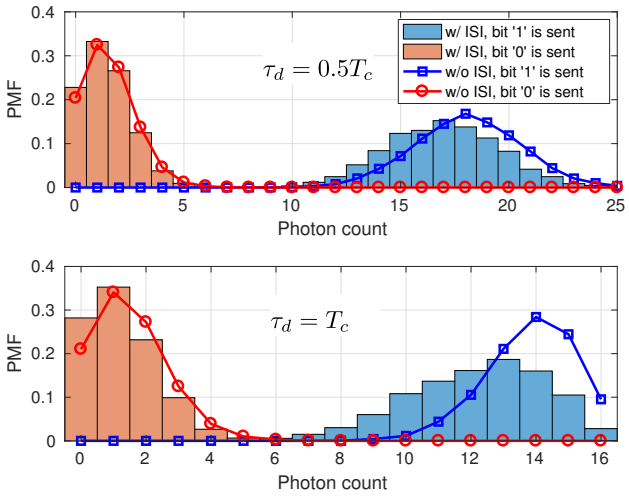

Fig. 2. The conditional PMF of the detected photon count for an AQ SPAD array with $N = 16$ in the presence and absence of ISI. OOK signal is transmitted. The symbol period is normalized and the photon rates (for each individual SPAD) for bit '1' and bit '0' transmission are 2 and 0.1, respectively.

Consider a symbol of counting period of length T_c that starts at the time $T_{\rm st}$ as shown in Fig. 1. In the presence of ISI, the SPAD is inactive at the beginning of the counting duration until the end of the pulse generated by the last photon arrived in the previous symbol. We denote this inactive period at the beginning of the current counting period as the *block time* $T_{\rm B}$. For AQ SPADs, $T_{\rm B}$ can be expressed as

$$T_{\rm B} = \max\left\{\tau_d - (T_{\rm st} - T_{\rm L}), 0\right\}, \tag{1}$$

where $T_{\rm L}$ is the last photon arrival time before the start of the counting period. Equation (1) indicates that with the information of the last photon arrival time available, the block time of the current symbol can be determined. On the other hand, for PQ SPADs, where the dead time is not fixed, $T_{\rm B}$ can be written only based on the falling edge, T_F, of the last pulse initiated in the previous counting period as

$$T_{\rm B} = \max\left\{T_{\rm F} - T_{\rm st}, 0\right\}. \tag{2}$$

In the presence of ISI, the SPAD is actually only active from $T_{\rm st} + T_{\rm B}$ rather than $T_{\rm st}$. Since both $T_{\rm L}$ and $T_{\rm F}$ are random variables, the ISI introduces a random inactive time which changes the statistics of the photon count during the considered symbol duration. In practical systems, SPAD arrays are commonly employed to improve the dynamic range and mitigate the saturation issue of such sensitive receivers at the expense of a lower fill-factor and hence less photon detection efficiency (PDE). Similar to the case of single SPAD, ISI also influences the statistics of the total photon counts in an array. In Fig. 2, the effect of ISI can be observed by comparing the conditional PMFs of the received photon count in the presence and absence of ISI when NRZ OOK signals are transmitted. This simulation result is achieved by firstly generating a relatively long photon arrival sequence based on the theory of Poisson process. When dead time induced ISI is

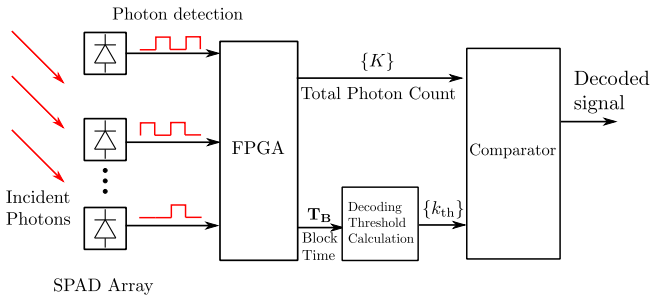

Fig. 3. The schematic of the proposed PTI-based detection technique.

considered, which is the case in practical scenario, this photon arrival sequence is filtered by dead time from the beginning to the end and the detected photon for each symbol is then counted. In contrast, when the dead time induced ISI is not considered, it is assumed that the SPAD is ready to collect photon at the beginning of each symbol. The original photon arrival sequence is filtered under this assumption and then counted. One can observe that with relatively small dead time, e.g., $\tau_d = 0.5T_c$, the PMFs of photon count in the presence of ISI deviate slightly from those in the absence of ISI. However, for a relatively large dead time, e.g., $\tau_d = T_c$, a significant mismatch between them are observed. This mismatch of PMFs is due to the fact that for longer dead time, the probability that the number of SPADs being inactive at the beginning of the current symbol increases. As a result, the ISI effect becomes more severe and the probability of detecting smaller photon counts increases. It is also demonstrated in Fig. 2 that the ISI results in smaller average value and larger variance of the detected photon count. These effects of ISI on the statistics of the detected photon count can significantly increase error probability in communication systems. Although large arrays of SPADs can be effective in combating ISI effects [3]–[5], ISI would still remain significant especially when the incident photon rate is high and/or when the dead time is comparable or longer than the symbol time. This is because the ISI induced by dead time is not only related to the dead time but also to the incident photon rate (both signal and background photon rates).

III. Optimal Detection Using Photon Time Information (PTI)

A. Receiver with Small SPAD Array

SPADs can provide both photon counts and accurate photon arrival times [13], [14]. Inspired by this capability, in this work we propose a new detection technique using both photon counts and their arrival times. We consider OOK modulation as an example, although the proposed idea can also be applied to systems with other modulation schemes.

The schematic of the proposed PTI-based detection scheme (PTID) is plotted in Fig. 3. The photon arrival sequences of the SPAD array are sent to the FPGA for extracting the total photon count and PTI. Using the PTI, the block time can be calculated based on (1) and (2) for AQ and PQ SPADs, respectively. Note that for the array-based receiver, the block times of SPAD elements are different from each other and hence a block time vector, $\boldsymbol{T_B}$, including the block times of individual SPADs, is required. The block time information is then used to calculate the decision threshold $k_{\rm th}$ and the signal is demodulated by comparing the photon count with $k_{\rm th}$. Different from the traditional system in the literature in which only photon count information is employed for communication and the decoding threshold is fixed, in our system the threshold for each symbol is calculated using the instantaneous block time information and is adapted to the instantaneous ISI status. Hence the degradation introduced by ISI effects can be minimized using such adaptive decision threshold. The proposed detection scheme requires that the receiver can provide the photon arrival pulse signals from each SPAD in the array. It is worth noting that such SPAD receiver has been practically realised as presented in [15].

For high-speed optical communication systems, in order to achieve higher data rates, it is very likely that the links are operated in the sub-dead-time regime where the symbol duration is equal or less than the dead time. In such sub-dead-time regime, a SPAD can at most detect one photon in a symbol duration. Therefore, the photon counting process becomes a Bernoulli process. For an array receiver, in the absence of ISI, the total photon count can be modeled as a Binomial distributed RV because of the identical probability of detecting a photon in every SPAD [16]. However, this is not the case in the presence of ISI, since each SPAD has different probability of detecting a photon. Considering the nth SPAD in the array, the conditional PMF of the photon count is given by

$$p_k(k|T_{{\rm B},n},\lambda)=\begin{cases}\exp\left[-\lambda\left(T_c-T_{{\rm B},n}\right)\right], & k=0,\\ 1-\exp\left[-\lambda\left(T_c-T_{{\rm B},n}\right)\right], & k=1,\end{cases} \tag{3}$$

where λ refers to the average received photon rate per SPAD. Thus, the total photon count of the SPAD array i.e.,

$$K=\sum_{n=1}^{N} k_n, \tag{4}$$

is the sum of Bernoulli RVs with different probabilities of success which are defined by the block time vector $\boldsymbol{T_B} = \{T_{{\rm B},1}, T_{{\rm B},2}, \cdots, T_{{\rm B},N}\}^T$. The total photon count K hence should follow the Poisson Binomial distribution with PMF

$$p_K(K|\boldsymbol{T_B},\lambda) = \sum_{\vartheta\in F_K}\prod_{i\in\vartheta}1-\exp[-\lambda\left(T_c-T_{{\rm B},i}\right)]\prod_{j\in\vartheta^c}\exp\left[-\lambda\left(T_c-T_{{\rm B},j}\right)\right], \tag{5}$$

where F_k is the set of all subsets of K integers that can be chosen from $\{1,2,\cdots,N\}$, N denotes the number of SPADs in the array, and ϑ^c is the complement of the subset ϑ. Note that the effect of ISI generally relates the likelihood statistics of each symbol to previous symbols. However, as explained earlier, the ISI effect due to dead time can be fully characterized by the vector $\boldsymbol{T_B}$; that is, $p_K(K|\boldsymbol{T_B},\lambda,\lambda^{(-1)},\lambda^{(-2)}\cdots,\lambda^{(-i)}) = p_K(K|\boldsymbol{T_B},\lambda)$ where $\lambda^{(-i)}$ denotes the photon rate of the symbol sent i symbol period before. Considering the Maximum-likelihood (ML) decoding, the system would decode the transmitted bit as '1'

when

$$p_K(K|\boldsymbol{T_B},\lambda_0) < p_K(K|\boldsymbol{T_B},\lambda_1), \tag{6}$$

holds where λ_0 and λ_1 denote the received photon rates per SPAD when bit '0' and bit '1' are transmitted, respectively, and decode the transmitted bit as '0' otherwise. The above ML decoding strategy can be simplified to a comparison between the detected photon count and a threshold. This optimal decision threshold $k_{\rm th}$ is given by the crosspoint of $p_K(K|\boldsymbol{T_B},\lambda_0)$ and $p_K(K|\boldsymbol{T_B},\lambda_1)$, which can be calculated numerically. Note that for data transmission with equiprobable messages the ML detector minimizes the probability of error [17]. The error probability conditioned on $\boldsymbol{T_B}$ can then be expressed as

$$\Pr(e|\boldsymbol{T_B}) = \frac{1}{2}\sum_{k=0}^{k_{\rm th}} p_K(K|\boldsymbol{T_B},\lambda_1) + \frac{1}{2}\sum_{k_{\rm th}}^{+\infty} p_K(K|\boldsymbol{T_B},\lambda_0). \tag{7}$$

The threshold $k_{\rm th}$ is adaptively determined by the instantaneous block time $\boldsymbol{T_B}$. This is similar to the signal detection in a fading channel where the detection threshold can be adaptively changed to minimise the BER performance based on the instantaneous fading status [18]. The average BER can be achieved by averaging the instantaneous error probability $\Pr(e|\boldsymbol{T_B})$ over the random $\boldsymbol{T_B}$.

B. Receiver with Large SPAD Array

Since the computational complexity of the Poisson Binomial PMF (5) increases dramatically with the increase of the array size N [19], the ML decoding based on this exact PMF is only applicable to small SPAD array. For those systems with large SPAD arrays, the approximation of the total photon count statistics based on the moment matching should be applied so that the decoding threshold $k_{\rm th}$ can be efficiently calculated. Invoking the PMF of the total photon count given in (5), the first two moments can be calculated as

$$\mu_K(\boldsymbol{T_B},\lambda) = \sum_{n=1}^{N} 1 - e^{-\lambda(T_c - T_{{\rm B},n})}, \tag{8}$$

$$\sigma_K^2(\boldsymbol{T_B},\lambda) = \sum_{n=1}^{N} \left[1 - e^{-\lambda(T_c - T_{{\rm B},n})}\right] e^{-\lambda(T_c - T_{{\rm B},n})}. \tag{9}$$

In the literature, different approximations of the Poisson Binomial distribution have been investigated such as Gaussian [19] and Binomial approximations [20]. Based on the moments given in (9), both of these two distributions can be employed to give analytical expressions of threshold $k_{\rm th}$ which significantly reduces the computational complexity. In the practical implementation, people can try both approximations and select the one with better performance. For OOK transmission considered in this work, the photon rate when bit '0' is sent is usually low due to the low background light intensity when proper optical filters are employed. In effect, the probabilities of receiving one photon at different SPADs of the array for bit '0' are small and are close to each other although not exactly equal due to ISI. It is known that when the probabilities of success are close to each other, the sum of the Bernoulli random variables can be accurately approximated as Binomial distribution [20]. As a result, Binomial distribution is a more suitable approximation to model the photon counts of bit '0' and hence is employed in the following discussion.

With Binomial approximation, the conditional PMF of the photon count (5) can be rewritten as

$$p_K^B(K;\boldsymbol{T_B},\lambda) = \binom{N}{k}\left[\frac{\mu_K(\boldsymbol{T_B},\lambda)}{N}\right]^k \left[1 - \frac{\mu_K(\boldsymbol{T_B},\lambda)}{N}\right]^{N-k}. \tag{10}$$

The analytical expression of the decoding threshold can be achieved by calculating the crosspoint of the two conditional PDF $p_K^B(K;\boldsymbol{T_B},\lambda_0)$ and $p_K^B(K;\boldsymbol{T_B},\lambda_1)$ which is given by

$$k_{\rm th}^{\rm B} = \frac{N \ln \frac{N-\mu_K(\boldsymbol{T_B},\lambda_1)}{N-\mu_K(\boldsymbol{T_B},\lambda_0)}}{\ln \frac{\mu_K(\boldsymbol{T_B},\lambda_0)(N-\mu_K(\boldsymbol{T_B},\lambda_1))}{\mu_K(\boldsymbol{T_B},\lambda_1)(N-\mu_K(\boldsymbol{T_B},\lambda_0))}}. \tag{11}$$

The signal detected can then be decoded by comparing the received photon count with the above threshold.

IV. Linear Channel Approximation

The effects of dead-time induced ISI in SPAD-based system is different from that in traditional communication systems. In traditional systems, in the absence of noise the current received symbol is simply the linear combination of the transmitted symbols [17]. As a result, the effect of channels can be described as a lowpass filter so that various equalization methods can be employed to compensate the lowpass effects. However, this is not the case in a SPAD based channel. As shown in (5), for a SPAD based receiver, the statistics of the detected photon count for each symbol duration is directly related to the instantaneous block time $\boldsymbol{T_B}$ rather than being linearly related to the previous transmitted symbols. Due to the random effect of block time $\boldsymbol{T_B}$, ISI acts as an additional source of noise. Moreover, even the average effect of ISI is nonlinearly related to the previous symbols due to the nature of dead time. Hence the channel itself cannot be expressed in a lowpass form and the commonly used equalizers designed for linear channels cannot achieve optimal performance in SPAD-based systems. In fact, they are only effective when the SPAD channel can be approximated as a linear one. Some works in the literature have shown the performance improvement of SPAD systems by employing the equalizers designed for traditional linear channels [5], [11], but none of them have investigated the reason why traditional equalizers can improve the performance of SPAD receiver. In this section, we discuss the conditions under which the SPAD channel can be approximated as a linear channel where the traditional equalization methods are effective.

In the absence of shot noise, the received signal is defined by the average detected photon count of the Poisson Binomial distribution in a symbol duration given in (8) as

$$\begin{aligned}\overline{K} &= \sum_{n=1}^{N} 1 - \exp\left[-\lambda\left(T_c - T_{{\rm B},n}\right)\right], \\ &= N - Ne^{-\lambda T_c}X,\end{aligned} \tag{12}$$

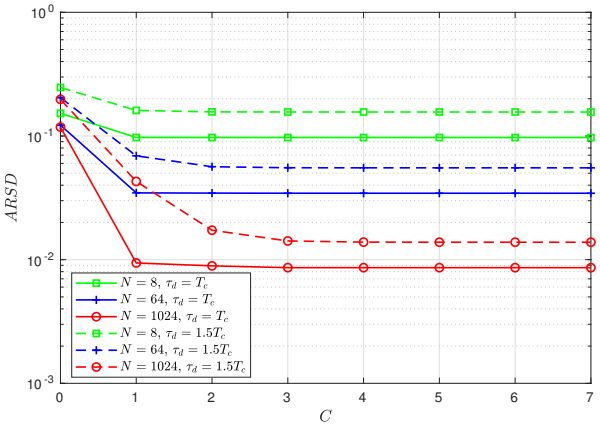

Fig. 4. The ARSD for systems with different SPAD array size and dead time where the received photon rates when bit '0' and bit '1' are sent are $\lambda_0 = 0.1/\tau_d$ and $\lambda_1 = 1/\tau_d + \lambda_0$, respectively.

where

$$X = \frac{1}{N}\sum_{n=1}^{N} e^{\lambda T_{\mathrm{B},n}}. \tag{13}$$

considering that the block time $T_{\mathrm{B},n}$ in (13) is random in general, $\overline{K}$ is a random variable. Therefore, even in the absence of shot noise, the SPAD channel is neither deterministic nor directly related to the transmitted symbols. However, in order to ensure that a linear equalization is applicable, a necessary condition is that $\overline{K}$ can be approximated as a deterministic function of the transmitted symbols. The level of randomness of $\overline{K}$ given the current and previous C transmitted symbols can be quantified using the so-called average relative standard deviation (ARSD). This metric is defined as the normalized standard deviation of $\overline{K}$ averaged over the 2^{C+1} possible combinations of the current and previously transmitted symbols and is given by

$$ARSD = \frac{1}{2^{C+1}}\sum_{i=1}^{2^{C+1}} \frac{\sigma_{\overline{K},i}}{\mu_{\overline{K},i}}. \tag{14}$$

where $\sigma_{\overline{K},i}$ and $\mu_{\overline{K},i}$ refer to the standard deviation and mean of $\overline{K}$, respectively, for the ith combination. Smaller ARSD indicates that $\overline{K}$ is more deterministic under the given $C+1$ transmitted symbols. Ideally, $\overline{K}$ can be expressed as a deterministic function of transmitted symbols at relatively large C where ARSD approaches zero.

An example of the ARSD for SPAD receivers with different sizes of SPAD arrays and dead times is plotted in Fig. 4. One can see that with the increase of C, ARSD firstly decreases and then saturates but never equals to zero. This emphasizes that $\overline{K}$ cannot be expressed as a fully deterministic function of previous transmitted symbols and remains random while its statistics would be related to a limited number of previous transmitted symbols. It is also presented that ARSD reduces with the increase of N. This is because with larger N, the random block time is averaged over the SPADs which results in less randomness of X and hence more deterministic $\overline{K}$. This is similar to the application of receiver diversity in faded communication channels [18]. In addition, it is also shown in Fig. 4 that with the increase of the dead time to symbol duration (DTSD) ratio, the ARSD increases and larger value of C is required for the ARSD to be saturated. This is because for larger dead time or less symbol time, the effects of the random ISI becomes more significant. In summary, the average received photon count $\overline{K}$ can only be approximated as a function of the transmitted symbols on the condition of large SPAD array size and small DTSD ratio.

When $\overline{K}$ can be approximated as a deterministic function of transmitted symbols, one can employ some equalization techniques to mitigate the effect of ISI. The simplest and most commonly used equalization is the linear equalizer. Here we investigate the design of the linear equalizer in the SPAD based system and discuss its performance. Note that as mentioned above $\overline{K}$ is inherently not a linear deterministic function of the transmitted symbols, hence a linear equalizer might only be effective under some specific conditions. Denote the received photon count in the jth symbol is K_j. Passing the received signal through the equalizer with $C'+1$ weight taps, the estimation of the jth symbol is given by

$$\hat{I}_j = \sum_{i=0}^{C'} \alpha_i K_{j-i}, \tag{15}$$

where $\{\alpha_i\}$ with $i = 0, \cdots, C'$ are the tap weight coefficients. Ignoring the noise and random ISI, the expected received number of photons in the jth symbol duration is given by

$$I_j = N(1 - e^{-\lambda_j T_c}). \tag{16}$$

Hence the optimal weight coefficient $\{\alpha_i\}$ of the linear equalizer can be determined by mean-square-error (MSE) criterion. The MSE is expressed as

$$\psi = \mathbb{E}\left(I_j - \hat{I}_j\right)^2 = \mathbb{E}\left(I_j - \sum_{i=0}^{C'} \alpha_i K_{j-i}\right)^2. \tag{17}$$

It can be shown that ψ is a convex function with respect to the weight coefficients. Therefore, the optimal coefficients minimizing the MSE can be found by solving a set of linear equations

$$\frac{\partial \psi}{\partial \alpha_n} = 0, \text{ with } n = 0, \cdots, C'. \tag{18}$$

Based on (17) and after some algebraic manipulations, the equation set can be expressed as

$$\mathbb{E}\left[\left(I_j - \sum_{i=0}^{C'} \alpha_i K_{j-i}\right) K_{j-n}\right] = 0, \text{ with } n = 0, \cdots, C'. \tag{19}$$

To solve the equation set, we can rewrite it in a matrix form as [17]

$$\boldsymbol{\Phi}\boldsymbol{\alpha} = \boldsymbol{\zeta}, \tag{20}$$

where $\boldsymbol{\alpha} = [\alpha_0, \alpha_1, \cdots, \alpha_{C'}]^T$, $\boldsymbol{\Phi}$ is the $(C'+1)\times(C'+1)$ correlation matrix given by

$$\boldsymbol{\Phi} = \begin{bmatrix} \mathbb{E}(K_j K_j) & \mathbb{E}(K_{j-1} K_j) & \cdots & \mathbb{E}(K_{j-C'} K_j) \\ \vdots & \vdots & \ddots & \vdots \\ \mathbb{E}(K_j K_{j-C'}) & \mathbb{E}(K_{j-1} K_{j-C'}) & \cdots & \mathbb{E}(K_{j-C'} K_{j-C'}) \end{bmatrix}$$

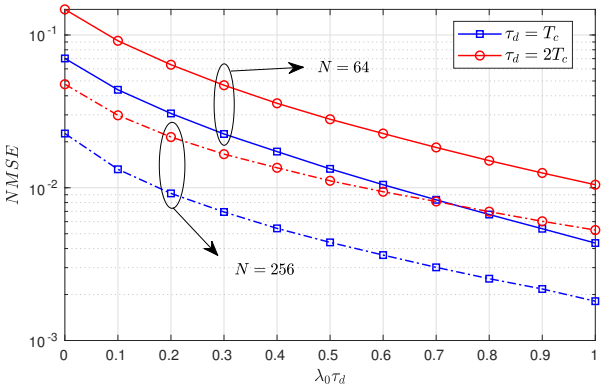

Fig. 5. The NMSE versus the background photon rate $\lambda_0\tau_d$ under different dead times and SPAD array sizes when $\lambda_1\tau_d = 0.4 + \lambda_0\tau_d$.

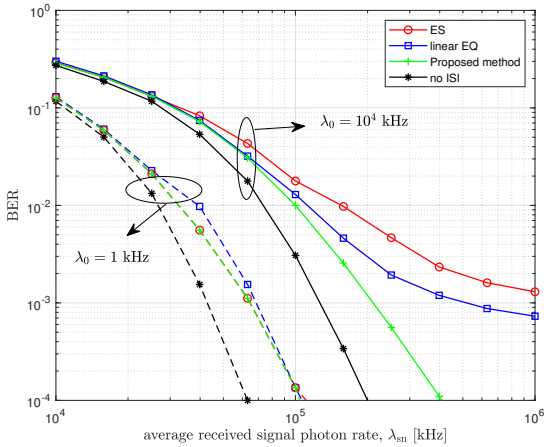

Fig. 6. The BER versus the average received signal photon rate per SPAD for the considered systems under various background photon rate where $N = 8$ and $\tau_d/T_c = 1.1$.

and the vector $\boldsymbol{\zeta}$ is given by

$$\boldsymbol{\zeta} = \left[\mathbb{E}\left(I_j K_j\right), \mathbb{E}\left(I_j K_{j-1}\right), \cdots, \mathbb{E}\left(I_j K_{j-C'}\right)\right]^T. \quad (21)$$

Note that both $\boldsymbol{\Phi}$ and $\boldsymbol{\zeta}$ can be achieved through numerical simulation. As a result, the optimal equalizer tap weights can be expressed as

$$\boldsymbol{\alpha}^* = \boldsymbol{\Phi}^{-1}\boldsymbol{\zeta}. \quad (22)$$

Fig. 5 shows an example of the normalized MSE (NMSE) denoted as $\psi/\mathbb{E}(I_j)^2$ versus the background photon rate under different dead times and array sizes. One can observe that with the increase of SPAD array size and the decrease of dead time, lower NMSE can be achieved which means that the equalizer can work more effectively under such conditions. This is mainly due to the less randomness of $\overline{K}$ given the previous transmitted symbols as mentioned above. In addition, it is also shown in Fig. 5 that with the increase of background light intensity, smaller NMSE is experienced as the SPAD channel is quite sensitive to the background light. When background light is small, the effect of the SPAD channel to bit '0' differs more from that to bit '1' and hence the channel becomes more non-linear. As a result, using a single linear filter to equalize the channel effect becomes less effective.

In summary, Our numerical results show that the traditional equalization methods designed for linear channel can be most effective in SPAD-based systems under the following conditions: the size of the SPAD array is large; the dead time to symbol duration is small; and the background light intensity is relatively large. It is worth noting that although the performance of traditional equalization is worse than that of the proposed detection technique (as shown later in Section V ans Section VI), its advantage lies in its simplicity. Therefore, when the SPAD channel can be approximated as a linear one, applying such linear equalization techniques is more suitable.

V. Numerical Results

We first present some simulation results to show the advantage of our proposed detection scheme over the state of the art. Four systems are considered in the simulation study. The first system refers to the ideal system considering dead time but ignoring the ISI effect. The second system (denoted as the system with ES) considers the ISI effect and uses a fixed decision threshold, determined by exhaustive search based on the histogram of the received photon count over all possible symbol transmissions, to minimize the BER. This demodulation method is widely used in experimental works in the literature [4]. However, the drawback of such system is that a long pilot signal should be transmitted to establish the accurate photon count histogram. For a real-time communication link with stochastic channel status (e.g., free-space optical communication through turbulent atmosphere), the histogram needs to be measured repeatedly every channel coherence time which might significantly reduce the effective transmission rate. The third system (denoted as linear EQ) refers to the one employing the linear equalization discussed in the last section. In this work, the tap weight coefficients of the equalizer is calculated based on (22) with $C' = 30$. Alternatively, some practically used adaptive linear equalizers based on various algorithms such as least mean squares (LMS) and recursive least squares (RLS), or DFE equalizer can also be used although they demonstrate similar performances based on our investigations. In Section VI, we demonstrate this point by including the performance of a DFE equalizer as an additional benchmark. Note that for system with linear EQ, the decoding threshold is still determined through exhaustive search which results in the minimal BER. However, different from the system with ES where the exhaustive search is directly applied to the histograms of the received photon counts, for systems with linear EQ the search is applied to the signals after equalization. The fourth system refers to the one employs the proposed PTID technique using PTI as shown in Fig. 3. The employed SPAD is assumed to be actively quenched and the dead time τ_d is set as 10 ns.

Figure 6 shows the BER performance of the considered four systems with respect to the average received signal photon rate per SPAD λ_{sn} for a small SPAD array with $N = 8$. Note that by definition the received photon rate is $\lambda_1 = 2\lambda_{\text{sn}} + \lambda_0$ and λ_0 when bit '1' and bit '0' are sent, respectively, where λ_0 denotes the background light photon rate. It is clear that even under

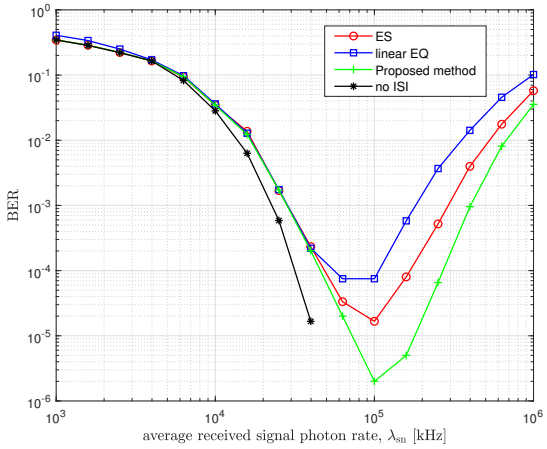

Fig. 7. The BER versus the average received signal photon rate per SPAD for the considered systems where the background photon rate is $\lambda_0 = 10^3$ kHz, $N = 256$ and $\tau_d/T_c = 10$.

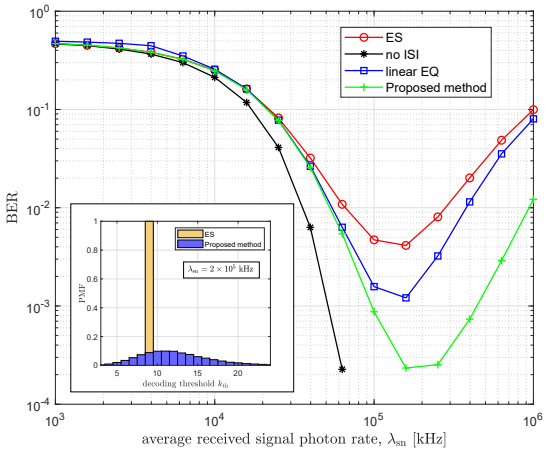

Fig. 8. The BER versus the average received signal photon rate per SPAD for the considered systems where the background photon rate is $\lambda_0 = 3 \times 10^4$ kHz, $N = 256$ and $\tau_d/T_c = 10$. The inset figure shows an example of the decoding threshold histogram.

very weak background photon rate $\lambda_0 = 1$ kHz, the system operates in the absence of ISI outperforms the other three in the presence of ISI, which reveals that the degradation caused by ISI is non-negligible when the dead time increases just beyond the symbol duration even under such weak background light intensity. Also, it is shown that the system with ES is similar to that with the proposed optimal detection technique and both perform better than that with the linear equalization. This is mainly due to the small SPAD array size and weak background light intensity as mentioned in Section IV. When significant background light is considered, e.g., $\lambda_0 = 10^4$ kHz, ISI effects become more severe and the performance of all systems are degraded. Hence, the advantages of the system with the proposed technique over the system with ES becomes obvious now. One can see that under such background light intensity, for the system with proposed scheme, an average signal photon rate of 2×10^5 kHz (1.81 photons/bit/SPAD) is required to achieve a BER of 1.3×10^{-3}; whereas for the system with ES, the corresponding required signal photon rate increase to 10^6 kHz (9 photons/bit/SPAD). Hence a 7 dB increase of receiver sensitivity can be achieved by using the proposed scheme. With the increase of the signal photon rate, higher sensitivities are expected to be achieved. In addition, the performance of the system with traditional linear equalization now becomes better than that of the ES; however, it is still worse than that of the proposed system. This is because although higher background light is considered here which is beneficial to the linear approximation of the SPAD channel as explained in the last section, the small size of the SPAD array still prohibits the effectiveness of the linear equalization.

Fig. 7 and Fig. 8 plot the corresponding BER performance for a SPAD receiver with a much larger array ($N = 256$) under various background light intensities. With such a large SPAD array, the receiver is more tolerant to the ISI introduced by dead time. Therefore, we can select a large DTSD ratio, e.g., $\tau_d/T_c = 10$, to boost the data rate. Considering a dead time of 10 ns, this ratio indicates that the system operates at a data rate of 1 Gbit/s. However, in this scenario since calculating the exact PMF of the Poisson Binomial distribution (5) is computationally complicated, we employed the approximated decoding threshold (11) to demodulate the signal. Note that if the Poisson Binomial PMF can be efficiently calculated based on which the optimal demodulation threshold can be achieved, the BER performance using our proposed system would be even better than the one shown in these two figures. As presented in Fig. 7, with relatively weak background light intensity, i.e, $\lambda_0 = 10^3$ kHz, the performance of the proposed system is comparable to that with ES in low average signal photon rate regime; however, with the increase of average signal photon rate, the proposed system outperforms that with ES. In addition, the performance of the system with equalization performs even worse than that with ES. This is because although here a large SPAD array is considered, due to the weak background light intensity, the SPAD channel is far from linear and hence equalization is not effective as mentioned in Section IV. Note that for all of the systems considering ISI, with the increase of $\lambda_{\rm sn}$, the BER firstly decreases and then increases. This is because in small $\lambda_{\rm sn}$ regime, increasing signal power increases average received signal when pulse signal is sent which improves the BER performance; however, large $\lambda_{\rm sn}$ also results in stronger ISI and higher probability of complete blockage when pulse signal is sent. As a result, the BER performance tends to increase when signal photon rate increases beyond a specific threshold. Similar behaviour can also be observed for systems with small SPAD array. In practical systems, one should keep the signal photon rates below such threshold to get a decent BER performance whereas using less transmitted power. In fact, the asymptomatic BER performance in high $\lambda_{\rm sn}$ for SPAD array is close to that of the system with single SPAD.

Under stronger background light intensity, i.e., $\lambda_0 = 3 \times 10^4$ kHz, the performance of all the systems considered are degraded as shown in Fig. 8. However, in this scenario the system with equalization outperforms that with ES in most of the

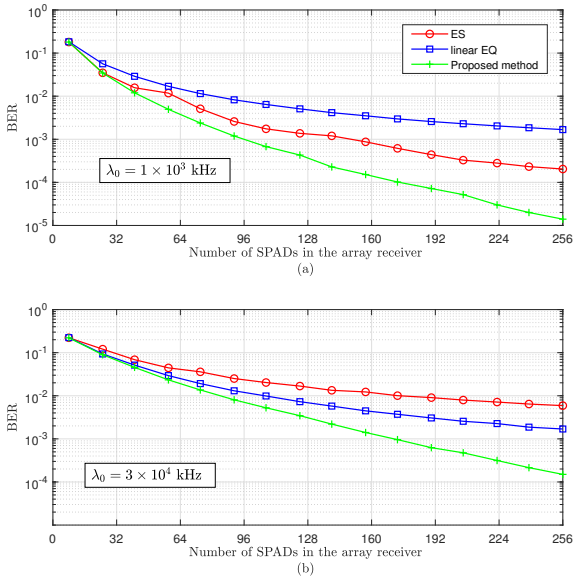

Fig. 9. The BER versus the number of SPADs in the array for considered systems under various background light intensities where $\lambda_{\rm sn} = 2 \times 10^5$ kHz and $\tau_d/T_c = 10$.

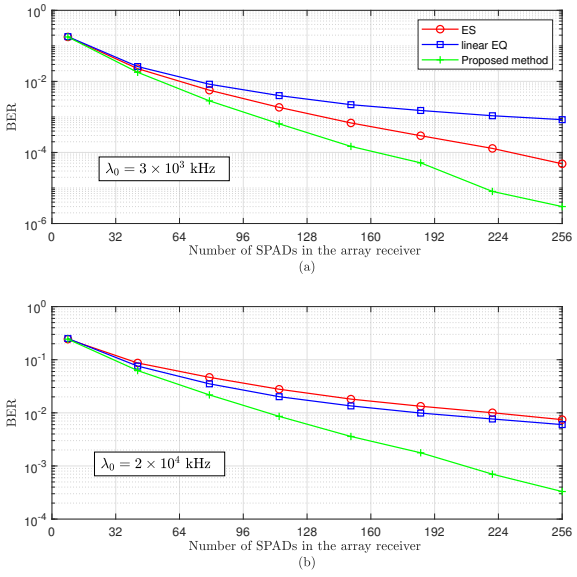

Fig. 10. The BER versus the number of PQ SPADs in the array for considered systems under various background light intensities where $\lambda_{\rm sn} = 7 \times 10^4$ kHz and $\tau_d/T_c = 5$.

considered range of signal photon rate thanks to the stronger background light intensities which makes the linear approximation of the SPAD channel more accurate. For instance, when $\lambda_{\rm sn}$ is 1.6×10^5 kHz (0.16 photons/bit/SPAD), the BER of the system with equalization is 1.2×10^{-3} whereas the corresponding BER for system with ES increases to 4×10^{-3}. In addition, the system with the proposed detection scheme always outperforms its counterparts. For example, under the aforementioned signal photon rate, the BER of the proposed system is only 2.3×10^{-4}. If a BER threshold of 10^{-3} is considered, both ES and linear EQ fail to achieve this requirement and only the proposed detection scheme can satisfy this requirement by choosing an average signal photon rate of 10^5 kHz. Therefore, the proposed system can efficiently improve the resilience of the receiver to the background light. In addition, the inset of Fig. 8 plots an example of the decoding threshold histogram for ES and the proposed scheme. One can observe that ES method selects a fixed decoding threshold determined by the photon counting statistics; however, in the proposed method, by further involving the PTI, the optimal decoding threshold can be calculated which changes symbol-by-symbol.

Figure 9 shows the BER versus the size of array in a AQ SPAD receiver for the considered systems under two aforementioned background light intensities. It is presented that with the increase of SPAD array size, better BER performance can be achieved. For a specific target BER, the proposed detection method requires a significantly smaller SPAD array size than the benchmark schemes. For instance, when $\lambda_0 = 10^3$ kHz, in order to achieve a BER of 10^{-3}, with our proposed method only 96 SPADs is required; however, the corresponding required SPAD sizes increase to 140 and 256 for systems with ES and linear EQ, respectively.

Although all of the above numerical results are based on the AQ SPAD receiver, the proposed method can also be applied for the receiver with PQ SPADs by using (2) to determine the block time vector. Accordingly, Fig. 10 shows the BER performance of PQ SPAD receivers versus the size of the receiver array. Note that because PQ SPAD is paralyzable and hence performs worse than AQ SPAD, in this figure a lower DTSD ratio 5 is considered to avoid excessive ISI effect. Fig. 10 shows that, compared to the results of AQ SPAD receiver, a relatively larger gain is observed for the proposed method compared to its counterparts. This is because PQ SPADs inherently experience more ISI induced by the dead time, which can be more effectively mitigated by the proposed detection method. In the next section, a more comprehensive performance analysis of PQ SPAD receivers will be presented using both numerical and experimental results.

Finally, in order to provide some insights on the improvement of achievable data rate by using the proposed PTI-based detection scheme, the achievable data rate and maximum DTSD ratio versus the number of SPADs in the array is plotted in Fig. 11. In this figure, AQ SPAD is considered and a relatively high background and signal light intensity is selected so that the dead time induced ISI effect is significant. A target BER of 10^{-3} is employed and the considered DTSD is restricted to a range from 1 to 20 with small discrete steps. For each SPAD array size, the maximum DTSD ratio satisfying the BER target is recorded. From Fig. 11, it is shown that for different considered detection methods, with the increase of array size, larger DTSD (or equivalently larger data rate) can be achieved. In addition, it is also presented that in order to achieve higher DTSD ratio a larger array size is required, as expected. The system with ES is strongly affected by the excessive dead time induced ISI and the data rate improvement

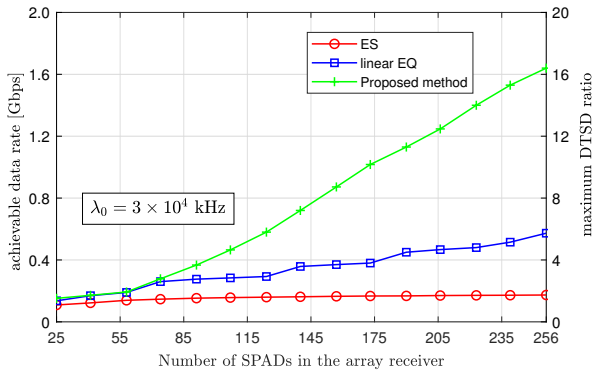

Fig. 11. The achievable data rate and maximum DTSD ratio versus the number of SPADs in the array for considered systems under a target BER of 10^{-3} where $\lambda_0 = 3 \times 10^4$ kHz and $\lambda_{\rm sn} = 2 \times 10^5$ kHz.

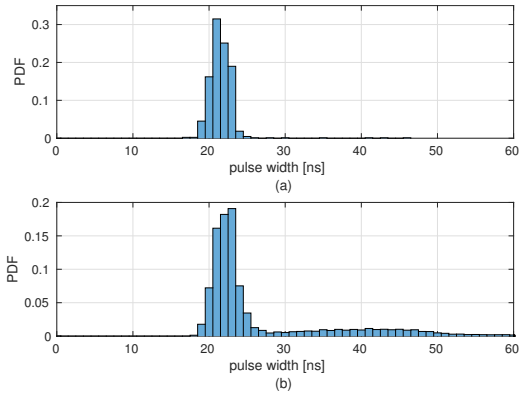

Fig. 12. The PDF of the pulse width under (a) weak light intensity and (b) relatively stronger light intensity.

through the increase of array size is quite limited. Even with the $N = 256$, the maximum DTSD ratio is only 1.74 which corresponds to an achievable data rate of 174 Mbps for a considered dead time $\tau_d = 10$ ns. The achievable data rate can be increased by using linear EQ or the proposed PTI-based detection scheme. However, the proposed method significantly outperforms linear EQ due to its better capability of mitigating the dead time induced ISI. For instance, with $N = 256$ a maximum DTSD ratio of 5.73 can be achieved by using linear EQ which refers to a data rate of 573 Mbps, but by employing the proposed method, the DTSD ratio can increase to 16.4 which corresponds to a data rate 1.64 Gbps.

VI. Experimental Results

In this section, we implement our proposed detection scheme experimentally using the passive-quenched SPAD receiver presented in [15]. In the test SPAD chip, the SPAD pitches vary from 8 μm to 30 μm are available. A maximum number of 128 SPAD digital outputs with 1 GHz sampling rate connected to the Xilinx Kintex-7 FPGA can be read out simultaneously. For each output signal, every rectangular pulse refers to a detected photon arrival and the minimal pulse width refers to the dead time under which the SPAD is inactive. In this work, the SPAD array with pitch size 15 μm and fill factor 60% is considered and a sub-array of 112 SPADs is employed for communication. The PDF of the pulse width of 112 outputs under two different incident light intensities is shown in Fig. 12. It is presented that under weak light intensity (Fig. 12(a)), the average pulse width is around 21 ns which indicates that the considered SPAD array has an average dead time of 21 ns. For passive quenched SPAD, any photon arriving during the dead time would extend the dead time, therefore longer pulse width can be observed when the light intensity becomes stronger as shown in Fig. 12(b).

The schematic diagram of the experiment setup is shown in Fig. 13. A 635 nm red LED is driven by a Keysight 33600A waveform generator which generates an analogue 60 Mbps unipolar OOK signal with rectangular pulse shaping. The SPAD photon detection probability (PDP) at this wavelength is 14.4% [21]. Considering that the symbol duration is $T_c = 16.7$ ns, the system is operated in the sub-dead-time regime with a DTSD ratio of 1.26. The experiment is operated in dark condition. Besides the LED transmitting signal, another 635 nm LED is employed in the setup as a background light source to provide variable ambient light intensity. Both signal and ambient lights are received by the SPAD receiver and the optical power is also measured by a power meter. The 112 digital output of the FPGA is sent to the computer for the offline signal processing, where the rising edges of each output can be extracted to get the photon count signal of each SPAD. The aggregated photon count signal can then be determined by combining all of the count signals together. It is worth noting that the above method of achieving the aggregated signal is equivalent to the OR tree combination but with an ideal pulse shortener [22]. Since in this method there is no loss of counts due to the combining network, the achieved performance outperforms the other systems with more practical combining techniques. By using the aggregated photon count signal and after synchronisation, the detected photon count within each symbol duration can be achieved by summing the photon counts in each symbol time. The BER performance of the considered traditional demodulation schemes using either the exhaustive search or the equalization can then be measured. To be in line with other SPAD-based experimental works where the DFE equalization is employed [11], [23], besides the linear equalizer the performance of the DFE equalizer is also presented in this section as an additional benchmark. The RLS algorithm is employed for the DFE equalizer and the number of feedforward and feedback weights are 41 and 15, respectively.

In order to measure the performance of the proposed detection scheme for PQ SPADs, besides the rising edge information, the falling edge information of the digital outputs should be also extracted from which the block time vector can then be obtained using (2). Since the LED used in the setup is only with a 3-dB bandwidth of around 20 MHz, the generated electrical OOK signal is strongly influenced by the LED low-pass frequency response and the pulse shape of the received signal at the SPAD receiver is far from the transmitted rectangular pulse shape. As a result, when a pulse symbol

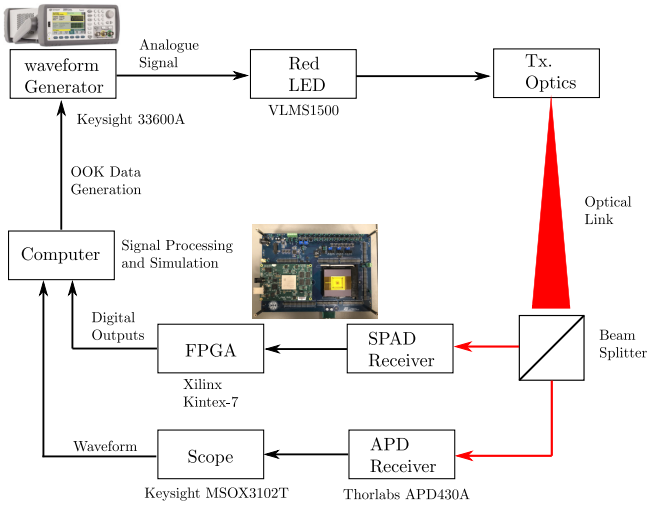

Fig. 13. The schematic diagram of the experiment setup.

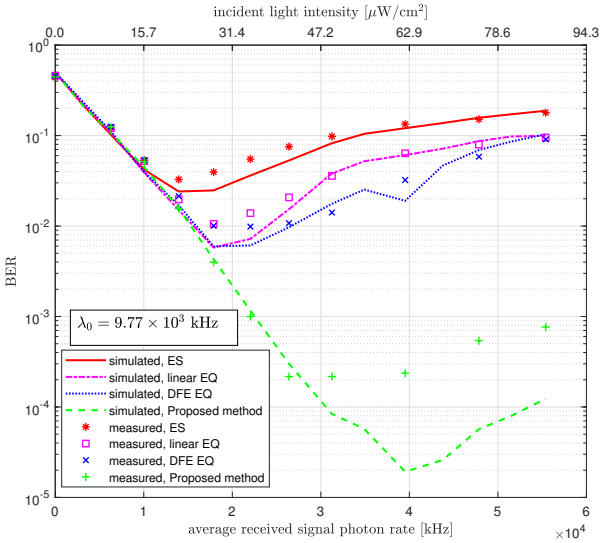

Fig. 14. The measured and simulated BER versus the average received signal photon rate per SPAD (bottom x-axis) and the corresponding incident light intensity (top x-axis) at a data rate of 60 Mbps. An array of 112 SPADs is employed and the measured background light intensity is 15.36 μW/cm^2 which refers to a photon rate of $\lambda_0 = 9.77 \times 10^3$ kHz.

is sent, the photon rate λ_1 is not fixed during each symbol time and across different symbols as assumed in the previous discussion. In this case, we can consider a range of λ_1 and use the λ_1 in (6) that minimizes the BER based on an initial pilot transmission before communication. Note that if the employed light source is with relatively large bandwidth compared to the signal bandwidth, e.g., laser source, this non-constant photon rate issue is negligible and the searching of the optimal photon rate for the calculation of threshold can be avoided.

To justify the measured BER performance, the corresponding simulation results with the same parameter settings should be presented. To make sure that the LED low-pass frequency response is also accurately involved in the simulation, a 50:50 non-polarizing beam splitter cube is utilised in this experiment as shown in Fig. 13 to illuminate a Thorlabs APD 430A with the signal light and a Keysight MSOX3102T scope is employed to record the signal optical waveform. The recorded signal optical waveform is sent to the computer to generate the simulation result. Since the recorded optical waveform suffers from the shot and thermal noise from the APD receiver, it is averaged for 30 times before sending the computer to suppress these noises. At the computer, the recorded waveform is then properly scaled so that its average optical power matches with that received by the SPAD receiver. With the estimated optical waveform at hand, the Poisson process can be used to simulate the photon arrival seen by the SPAD. It is worth noting that if the accurate frequency response and the relationship between the optical intensity and forward voltage of the LED are available, it is possible to generate the optical waveform received by the SPAD receiver through pure simulation rather than using the above compromised method.

Fig. 14 plot the measured and simulated BER performance for different systems versus the signal photon rate (bottom x-axis) and the incident light intensity (top x-axis) when the background light intensity is 15.36 μW/cm^2 which corresponds to a photon rate of 9.77×10^3 kHz to each SPAD. The performances of the two systems with equalizers are quite close. From both measured and simulated results, it is demonstrated that, comparing with the traditional schemes, the proposed detection method can achieve a significant BER improvement for PQ SPADs. For instance, based on the measurement, although the systems with equalizers can achieve better BER performance compared to the one with ES, their minimum achievable BER is only around 10^{-2}. However, the proposed system can achieve a BER below 10^{-3} when the signal photon rate (light intensity) is between 2.2×10^4 kHz (34.6 μW/cm^2) and 5.54×10^4 kHz (87.1 μW/cm^2). One can also observe that generally the simulated results outperform that of the measured ones. This is mainly due to the limited FPGA sampling rate of the SPAD receiver which is not considered in the simulation. Since the proposed system utilises the photon arrival time for decoding, it is more sensitive to the limited sampling rate. Therefore, a relatively larger gap between the simulated and measured results can be seen.

In Fig. 15 the measured BER performance under a weaker background light intensity 8.06 μW/cm^2 is also presented. Due to the less background photon rate, better BER performance for all systems compared to Fig. 14 can be observed. This weaker background light also causes the SPAD channel to become more non-linear which results in the performance of linear EQ inferior to that of ES in high signal photon rate regime. The experimental result shows that none of the traditional schemes can achieve a BER below 10^{-3} over the considered range of the signal photon rates; whereas, for the proposed system when the signal photon rate is above 1.79×10^4 kHz (28.1 μW/cm^2), a BER below 10^{-3} can always be guaranteed and BER values as low as 1.6×10^{-5} can be achieved. From Fig. 14 and Fig. 15, the sensitivity of the employed SPAD receiver with the proposed detection technique can also be calculated. When the background light intensity is 8.06 μW/cm^2, considering a BER target of below

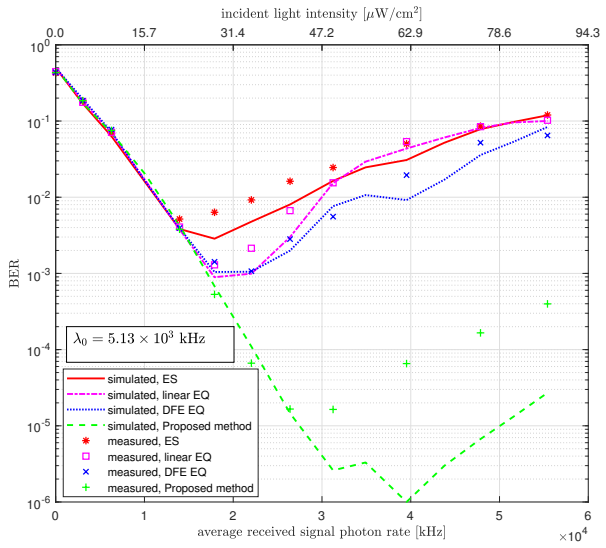

Fig. 15. The measured and simulated BER versus the average received signal photon rate per SPAD (bottom x-axis) and the corresponding incident light intensity (top x-axis) at a data rate of 60 Mbps. An array of 112 SPADs is employed and the measured background light intensity is 8.06 μW/cm^2 which refers to a photon rate of $\lambda_0 = 5.13 \times 10^3$ kHz.

10^{-3}, a sensitivity of -51.42 dBm is achieved, which is similar to the -51.2 dBm sensitivity reported in the work [2] for 50 Mbit/s NRZ OOK signal transmission with a higher BER target of 2×10^{-3} and in dark conditions. The sensitivity of the considered system can be significantly improved by operating the system in dark environment and by reducing the dead time. Measuring the highest sensitivity and the achievable data rate of the proposed SPAD based scheme will be the subject of a future work.

VII. Conclusion

In this work, the effect of dead-time-induced ISI on SPAD-based optical wireless communication systems is investigated. A novel detection technique is designed to mitigate the performance degradation caused by ISI in which the PTI is incorporated to provide an optimal detection scheme. By comparing the proposed PTI-based detection scheme with the state-of-the-art schemes, it is demonstrated that the proposed scheme significantly improves BER and achievable data rate, which effectively enhances the tolerance of the SPAD-based receiver to the background light. In particular, it is demonstrated that when background and signal photon rates are 3×10^4 kHz and 2×10^5 kHz, respectively, with an array of 256 SPADs and a target BER of 10^{-3}, the proposed PTI-based scheme can achieve a data rate of 1.64 Gbps; whereas, the corresponding data rate when the linear equalizer is employed is only 573 Mbps. In addition, the linear approximation of the SPAD channel is investigated. It is demonstrated that only under some specific conditions, the channel can be effectively equalized using a linear model. Finally, the superiority of our proposed scheme is demonstrated through experimental results.

VIII. Acknowledgements

We gratefully acknowledge the financial support from EPSRC under grant EP/R023123/1 (ARROW). We also thank STMicroelectronics for the fabrication of the integrated circuit.

References

[1] S. Huang and M. Safari, "Quantum limited optical receivers in the presence of intersymbol interference," accepted in 2019 European Conference on Optical Communication (ECOC).

[2] H. Zimmermann, B. Steindl, M. Hofbauer, and R. Enne, "Integrated fiber optical receiver reducing the gap to the quantum limit," *Scientific reports*, vol. 7, no. 1, p. 2652, 2017.

[3] E. Fisher, I. Underwood, and R. Henderson, "A reconfigurable single-photon-counting integrating receiver for optical communications," *IEEE Journal of Solid-State Circuits*, vol. 48, no. 7, pp. 1638–1650, July 2013.

[4] D. Chitnis and S. Collins, "A SPAD-based photon detecting system for optical communications," *J. Lightwave Technol.*, vol. 32, no. 10, pp. 2028–2034, May 2014.

[5] J. Kosman, O. Almer, T. A. Abbas, N. Dutton, R. Walker, S. Videv, K. Moore, H. Haas, and R. Henderson, "29.7 a 500Mb/s -46.1dBm CMOS SPAD receiver for laser diode visible-light communications," in *2019 IEEE International Solid- State Circuits Conference - (ISSCC)*, Feb 2019, pp. 468–470.

[6] S. Cova, M. Ghioni, A. Lacaita, C. Samori, and F. Zappa, "Avalanche photodiodes and quenching circuits for single-photon detection," *Appl. Opt.*, vol. 35, no. 12, pp. 1956–1976, Apr 1996.

[7] Y. Li, M. Safari, R. Henderson, and H. Haas, "Nonlinear distortion in SPAD-based optical OFDM systems," in *2015 IEEE Globecom Workshops (GC Wkshps)*, Dec 2015, pp. 1–6.

[8] ——, "Optical OFDM with single-photon avalanche diode," *IEEE Photonics Technology Letters*, vol. 27, no. 9, pp. 943–946, May 2015.

[9] F. Y. Daniel and J. A. Fessler, "Mean and variance of single photon counting with deadtime," *Physics in Medicine & Biology*, vol. 45, no. 7, p. 2043, 2000.

[10] E. Sarbazi, M. Safari, and H. Haas, "Statistical modeling of single-photon avalanche diode receivers for optical wireless communications," *IEEE Transactions on Communications*, vol. 66, no. 9, pp. 4043–4058, Sep. 2018.

[11] L. Zhang, D. Chitnis, H. Chun, S. Rajbhandari, G. Faulkner, D. O'Brien, and S. Collins, "A comparison of APD- and SPAD-based receivers for visible light communications," *J. Lightwave Technol.*, vol. 36, no. 12, pp. 2435–2442, Jun 2018.

[12] L. Zhang, H. Chun, Z. Ahmed, G. Faulkner, D. O'Brien, and S. Collins, "The future prospects for SiPM-based receivers for visible light communications," *J. Lightwave Technol.*, vol. 37, no. 17, pp. 4367–4374, Sep 2019.

[13] T. Al Abbas, N. A. W. Dutton, O. Almer, N. Finlayson, F. M. D. Rocca, and R. Henderson, "A CMOS SPAD sensor with a multi-event folded flash time-to-digital converter for ultra-fast optical transient capture," *IEEE Sensors Journal*, vol. 18, no. 8, pp. 3163–3173, April 2018.

[14] A. Griffiths, J. Herrnsdorf, C. Lowe, M. Macdonald, R. Henderson, M. Strain, and M. Dawson, "Temporal encoding to reject background signals in a low complexity, photon counting communication link," *Materials*, vol. 11, no. 9, p. 1671, 2018.

[15] S. Patanwala, I. Gyongy, N. Dutton, B. Rae, and R. Henderson, "A reconfigurable 40 nm CMOS SPAD array for LiDAR receiver validation," in *2019 International Image Sensor Workshop (IISW)*, Jun 2019, pp. 1–4.

[16] H. Mahmoudi, M. Hofbauer, B. Steindl, K. Schneider-Hornstein, and H. Zimmermann, "Modeling and analysis of BER performance in a SPAD-based integrated fiber optical receiver," *IEEE Photonics Journal*, vol. 10, no. 6, pp. 1–11, Dec 2018.

[17] J. Proakis, *Digital Communications*, ser. Electrical engineering series. McGraw-Hill, 2001.

[18] M. Safari, "MIMO free-space optical communication," in *Optical Wireless Communications*. Springer, 2016, pp. 231–253.

[19] Y. Hong, "On computing the distribution function for the poisson binomial distribution," *Computational Statistics & Data Analysis*, vol. 59, pp. 41–51, 2013.

[20] W. Ehm, "Binomial approximation to the poisson binomial distribution," *Statistics & Probability Letters*, vol. 11, no. 1, pp. 7–16, 1991.

[21] S. Pellegrini, B. Rae, A. Pingault, D. Golanski, S. Jouan, C. Lapeyre, and B. Mamdy, "Industrialised SPAD in 40 nm technology," in *2017 IEEE International Electron Devices Meeting (IEDM)*, Dec 2017, pp. 16.5.1–16.5.4.

[22] S. Gnecchi, N. A. W. Dutton, L. Parmesan, B. R. Rae, S. Pellegrini, S. J. McLeod, L. A. Grant, and R. K. Henderson, "Digital silicon photomultipliers with OR/XOR pulse combining techniques," *IEEE Transactions on Electron Devices*, vol. 63, no. 3, pp. 1105–1110, March 2016.

[23] Z. Ahmed, R. Singh, W. Ali, G. Faulkner, D. OBrien, and S. Collins, "A SiPM-based VLC receiver for Gigabit communication using OOK modulation," *IEEE Photonics Technology Letters*, vol. 32, no. 6, pp. 317–320, 2020.